Catalysis Today 423 (2023) 114013

Contents lists available at ScienceDirect

Catalysis Today

journal homepage: www.elsevier.com/locate/cattod

The selective ethanol Guerbet condensation over alkali metal-doped sepiolite

Giulia Balestra [a,b,c], Jacopo de Maron [b], Tommaso Tabanelli [b,c], Fabrizio Cavani [b,c,*], Josè Manuel López Nieto [a,**]

[a] Instituto de Tecnología Química, Universitat Politecnica de Valencia-Consejo Superior de Investigaciones Científicas, Avenida de los Naranjos s/n, 46022 Valencia, Spain

[b] Dipartimento di Chimica Industriale "Toso Montanari", Alma Mater Studiorum Università di Bologna, Viale Risorgimento 4, 40136 Bologna, Italy

[c] Center for Chemical Catalysis C3, Alma Mater Studiorum Università di Bologna, Italy

ARTICLE INFO

Keywords:
Ethanol
Guerbet reaction
Butanol
Gas-phase
Continuous-flow processes
Sepiolite
Heterogenous catalyst

ABSTRACT

In this study, alkali metal-doped sepiolite based catalysts were developed for the up-grading of ethanol through the Guerbet reaction mechanism. The catalysts were prepared by wetness impregnation with aqueous solution containing alkali metal precursors salts over calcined sepiolite, and finally activated at 500ºC in air. The catalysts have been characterized by XRD, SEM-EDS, TGA-DSC, N_2-adsorption. In addition, TPD-CO_2 and TPD-NH_3 were used to determine the acid and basic characteristics of catalysts. The catalysts were tested into a quartz continuous gas-flow reaction system working at atmospheric pressure to investigate the effects of metal loading (wt%), the nature of the alkali metals and of the main reaction parameters (e.g., reaction temperature, weight hourly space velocity), on the production of *n*-butanol starting from ethanol. The highest yield (18%) was obtained at 400 ºC with the catalyst consisting in sepiolite, calcined at 500ºC, impregnated with 7 wt% of Cs. This study proves that ad hoc modified natural sepiolites with alkali metals are effective catalysts for the Guerbet upgrading of ethanol.

1. Introduction

Fossil fuels (petroleum, natural gas, and coal) inevitable depletion and related adverse effects of their exploitation (e.g., the rising greenhouse gas concentrations in the atmosphere, global warming, ocean acidification and rising sea levels) led to the developments of new approaches toward production of fuels and chemicals [1]. In this regard, the use of renewable resources for the generation of energy and production of chemicals is considered a major imperative in the 21st century [1]. Among various biofuels, platform molecules and end-use products derived from biomass, bio-ethanol is the most important one [2]. Ethanol is currently mainly produced via biomass fermentation processes. The great majority of the bio-ethanol produced to date is still obtained by first generation biomass fermentation, particularly from starch and sugars [3,4]. But, in order to be truly sustainable, its production should not compete with food production. Therefore, many researches focused on the development of more efficient technologies starting from low-cost and non-food biomass sources, such as from lignocellulosic feedstock (second generation bio-ethanol) [5–11]. To date, bio-ethanol has dominated the bio-gasoline market, used on its own or as a blend with conventional fuels. However, ethanol is characterized by a relatively low vapor pressure, has a lower energy density (roughly 70% compared to traditional gasoline), it readily absorbs water leading to separation and dilution problems in storage tanks, and it is corrosive to current engine technology and fuel infrastructure. Bio-ethanol can be used as a 5% blend with petrol under the EU quality standard EN 228. This blend requires no engine modification and is covered by vehicle warranties. With engine modification, bio-ethanol can be used at higher levels, for example, E85 (85% bio-ethanol). Hence, limiting the amount of ethanol blended with gasoline presents several drawbacks that can be overcome by using higher alcohols with better fuel properties [12].

Accordingly, *n*-butanol is essentially noncorrosive, only slightly soluble in water, and its energetic value, i.e. the net heat of combustion

* Corresponding author at: Dipartimento di Chimica Industriale "Toso Montanari", Alma Mater Studiorum Università di Bologna, Viale Risorgimento 4, 40136 Bologna, Italy.

** Corresponding author.

E-mail addresses: fabrizio.cavani@unibo.it (F. Cavani), jmlopez@itq.upv.es (J.M.L. Nieto).

https://doi.org/10.1016/j.cattod.2023.01.020

Received 6 December 2022; Received in revised form 19 January 2023; Accepted 23 January 2023

Available online 24 January 2023

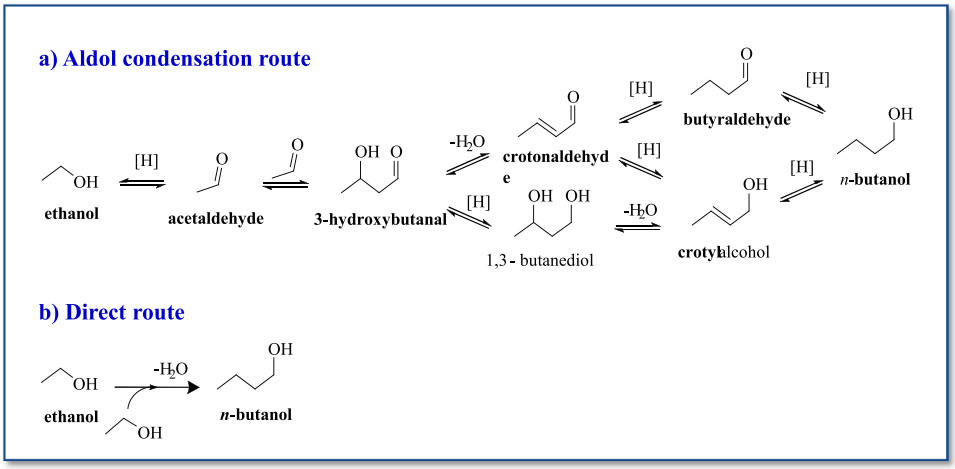

Scheme 1. Generally accepted pathway for ethanol upgrading through Guerbet routes to n-butanol.

(NHOC), is equal to 26.8 MJ/L, a value higher compared with the one of ethanol (21.1 MJ/L) and roughly 83% that of gasoline (32.3 MJ/L) [12–14]. This improved performance has led *n*-butanol to being inserted in the "advanced biofuel" list, and the commercial availability of this material as a green drop-in alternative to gasoline is gaining ground. Nevertheless, *n*-butanol is a valuable product with many applications as solvent, additive in many commercial products or as chemical intermediate, for instance is a crucial building block for acrylic acid and acrylic esters [14,15]. Its petrochemical-based route of synthesis, the so-called Oxo process, involves several reaction steps, some of which use homogeneous catalysts and non-renewable resources such as propylene and CO [14]. Bio-butanol can be obtained through the ABE (Acetone, Butanol and Ethanol) fermentation process, where this organic mixture is produced by the use of strains of the bacterium Clostridium acetobutylicum. However, it's a challenging fermentation process with relatively low conversion and modest selectivity [16,17]. An attractive alternative approach to obtain bio-butanol is to catalytically convert or upgrade widely available bio-ethanol through the so called "Guerbet reaction", which enables C-C bond formation between alcohols [18–23]. In addition, through the Guerbet route also higher alcohols (C_6-C_{12}) can be produced, mainly branched like 2-alkyl alcohols named "Guerbet alcohols" (i.e. 2-ethyl hexanol derived from the condensation of two *n*-butanol molecules). These can be considered an added benefit since higher alcohols have an appropriate energy density to be combined with gasoline (e.g., the energy densities of 1-hexanol and 1-octanol are the 94% and 99% of that of gasoline, respectively) [24], or to be employed in fuel blends for diesel engines [25].

The two main reaction mechanisms proposed in the literature for the Guerbet reaction are depicted in Scheme 1. The most accepted one, that is based on aldol condensation ("aldol-condensation route"), starts with the dehydrogenation of ethanol over basic or redox active sites producing acetaldehyde, commonly reported as the key intermediate. Acetaldehyde can then undergo to the aldol condensation to yield 3-hydroxybutanal (acetaldol). Then the reduction of the aldol can occur through the H-transfer mechanism from ethanol, the Meerwein–Ponndorf–Verley (MPV) reaction [26,27]. Nonetheless, the in-situ formed hydrogen (from ethanol dehydrogenation) might also play a role as reducing agent. The second one, the "direct route", involves the condensation of two ethanol molecules with no intermediate gaseous compounds over basic heterogeneous catalysts, which is suggested to occur by direct coupling of two ethanol molecules with dehydration occurring by the elimination of the hydroxyl of one molecule and the hydrogen attached to the α-carbon of the second one [28]. The actual mechanism is still under discussion, especially when ethanol-upgrading reaction is studied over heterogeneous basic catalysts, as shown by the presence of several alternative mechanisms proposed in the literature [29]. This variety is related to the different reaction conditions performed over different catalytic systems characterized by diverse physicochemical properties, so it's difficult to reach a universal conclusion [30].

A variety of homogeneous, homogeneous/ heterogeneous, and heterogeneous catalysts have been studied for the Guerbet reaction. Most of the homogeneous systems employed use basic catalysts such as alkaline catalysts or systems modified by homogenously or heterogeneously addition of a metal to accelerate the dehydrogenation and hydrogenation steps [31].

The realization of the continuous-flow, vapor-phase reaction opens new routes for industrial production of *n*-butanol from bio-ethanol. Indeed, performing the reaction in vapor phase allows higher temperatures to be reached without pressure build-up, which generally imposes practical limitations to liquid phase systems such as autoclave. At high temperatures, typically 350–450 °C, the basic catalyst can also catalyze the dehydrogenation reaction [28]. Therefore, there are many studies describing high temperature, vapor-phase reactions performed with catalysts devoid of transition metals as active phase. Indeed, the most studied heterogeneous catalyst by far is the basic magnesium oxide (MgO), which owing to its superior activity and selectivity has often been used as a reference catalyst for studying Guerbet mechanism [32–36]. Regardless, the Guerbet reaction has been studied over many different heterogeneous catalysts, including mixed metal oxides [37], hydrotalcite [38], cation exchanged zeolites [13] and supported metal catalysts.

Here we propose the use of the natural clay sepiolite as the basis for a heterogeneous catalyst for the ethanol Guerbet up-grading. Sepiolite is a hydrated Mg-rich silicate mineral belonging to the clay family [39]. Its molecular formula is $Mg_8Si_{12}O_{30}(OH)_4(H_2O)_4{\bullet}8\,H_2O$ and exhibits microfibrous morphology, showing an alternation of blocks and tunnels that grow up in the fiber direction and which can accommodate "zeolitic" water and other molecules (Fig. S1 in the electronic supporting information, SI) [39,40]. Each structural block is composed of two tetrahedral silica sheets linked by means of oxygen atoms to a central sheet of magnesium oxide-hydroxide, so that the tetrahedral sheet is continuous, but with the directions of the apical end of the silica tetrahedrons of the adjacent ribbons inverted. Theoretically, every octahedral site of the ideal sepiolite is occupied by Mg(II) cations; however, magnesium ions in sepiolite crystal are exchangeable with various transition metal ions [41,42]. This special crystal structures lead to a variety of physicochemical properties, such as expansion of the interlayer space, cation exchange, small particle size, high surface area, and so forth. They are naturally occurring, cheap, eco-friendly, nontoxic and abundantly available [43]. Thus, considering the "Green and Sustainable Development" concept, sepiolite gained both industrial and

academic attention [44].

In the present work, a series of natural sepiolite samples have been modified by calcination and impregnation with different alkali metals (i.e., Na^+, K^+ or Cs^+). All the sample have been in-depth characterized using the state of the art of different techniques. The main purpose of this study is to determine the effect of the alkali metals on the structures and acid/base properties of the produced materials correlating these properties to the observed catalytic performances in the Guerbet upgrading of ethanol to *n*-butanol.

2. Experimental

2.1. Materials

Natural sepiolite (Sepiolite 11AS-13) was provided by Tolsa, S.A. Reagents and standards were analytical grade, in particular: absolute ethanol (Scharlab), $Mg(CH_3COO)_2{\cdot}4\ H_2O$ (%), $HO_2CCO_2H{\cdot}2\ H_2O$ (99%), Na_2CO_3 (99.8%), K_2CO_3 (99%), Cs_2CO_3 (99%) all obtained from Sigma Aldrich and used as received.

2.2. Preparation of the catalysts

Magnesium oxide was synthesized by precipitation method [45]. The precipitation has been conducted at pH 5 with a NH_4OH 1.3 M aqueous solution, of a magnesium acetate $Mg(CH_3COO)_2{\bullet}4\ H_2O$ solution with an oxalic acid $C_2O_4H_2{\cdot}2\ H_2O$ solution, in which the magnesium oxalate β-MgC_2O_4 precipitate immediately. The solid obtained was filtered, washed, and dried at 80ºC overnight. The obtained solid has been calcined at 700 ºC for 3 h, with a 2 ºC min^{-1} ramp, obtaining the magnesium oxide MgO.

Sepiolite catalysts were prepared starting from a sample of natural sepiolite, previously calcined at 500ºC or 700 °C. Sepiolite supports have been impregnated with alkali metals (i.e., Na, K and Cs) by incipient wetness impregnation (IWI). To do so, an appropriate amount of aqueous metal carbonate solutions has been added drop-wise to the calcined sepiolite after a previous measure of the mud point of the support. A slurry has been obtained and the powdery solid was manually mixed in order to accomplish the maximum homogeneity. Then, the solids were dried at 100 ºC (16 h) and calcined in air at 500 ºC for 3 h with a heating ramp of 2 ºC min^{-1}. The general symbols for the catalysts used were xM/Sep@Y, where "x" was the number related to the metal amount (2, 4, 5, 7 or 14) expressed as weight percent (wt%), "M" the alkali metal concerned (Na, K or Cs) and "Y" the calcination temperature employed for the sepiolite support (i.e. 500 or 700 ºC).

In particular, the following catalysts have been synthesized:

- xNa/Sep@ 500 series (with 2 or 5 wt% of Na^+) and xNa/Sep@ 700 series (with 2 or 5 wt% of Na^+);
- xK/Sep@ 500 series (with 2 or 5 wt% of K^+);
- xCs/Sep@ 500 series (with 2, 4, 7 or 14 wt% of Cs^+).

Before performing the reactions, all the calcined samples have been shaped into 0.25–0.6 mm pellets. To do so, the powder was pressed into a self-sustaining disk (≈1 mm in height and 3 cm in diameter), which was then crushed using appropriate sieves.

2.3. Catalyst characterization

The XRD powder patterns of all materials were acquired using a PANalytical X'Pert PRO equipped with a Cu Kα radiation and an X'Celerator detector in Bragg-Brentano operating at 40 keV and 30 mA.

The specific surface area (S_{BET}) of catalysts were obtained from N_2 adsorption isotherms using a Micromeritics ASAP 2000 instrument. Samples were degassed in situ, under vacuum, at a 250 °C temperature. The specific surface areas were calculated by the Brunauer–Emmett–-Teller (BET) method and pore volumes were obtained by the Barrett–Joyner–Halenda (BJH) method.

Ammonia temperature programmed desorption (TPD-NH_3) were carried out with a TPD/2900 apparatus from Micromeritics. 30 g of sample were pre-treated in an Ar stream at 350 °C for 1 h. Ammonia was chemisorbed by pulses at 100 °C until equilibrium was reached. Then, the sample was fluxed with a He stream for 15 min, prior to increasing the temperature up to 500 °C in a helium stream of 100 mL min^{-1} and using a heating rate of 10 °C min^{-1}. The NH_3 desorption was monitored with a thermal conductivity detector (TCD) and a mass-spectrometer following the characteristic mass of ammonia at 15 a.m.u.

Carbon dioxide temperature programmed desorption (TPD-CO_2) experiments were performed in an Autochem II (Micrometrics) instrument with catalyst in pellets (calcined) for the analysis of the base properties of catalyst. The sample was placed in a quartz tubular reactor and pre-treated under 30 mL min^{-1} He flow to the calcination temperature (500 °C) for 60 min, in order to remove adsorbed H_2O and CO_2 from the catalyst surface prior to adsorption. Then the catalyst was cooled down to 40 °C and the catalyst surface was saturated with the probe molecule for 1 h (flow rate of 30 mL min^{-1} of 10 v/v % of CO_2 in He). Physisorbed CO_2 was removed by flowing He (30 mL min^{-1}) for 60 min. Then, the sample was heated at 10 °C min^{-1} up to 500 °C and the desorbed probe molecules were monitored and recorded using TCD detector.

Morphological and structural characterization of the samples was performed by scanning electron microscopy (SEM) and energy-dispersive spectrometry (EDS). Scanning electron microscopy (SEM) micrographs were collected in a JEOL 6300 microscope operating at 20 kV. The quantitative EDX analysis was performed using an Oxford LINK ISIS System with the SEMQUANT program. In this work, Energy Dispersive Spectroscopy was used to perform a semi-quantitative analysis of the elements, in particular to quantify the alkali-metals amount.

TGA analyses of catalysts were performed on NETZSCH STA 449 F3 Jupiter® that permits the simultaneous measurement of weight changes and thermal effects. The sample (typically 10 mg) was heated up to 800 °C with a heating rate of 10 °C min^{-1} in air flow (100 mL min^{-1}).

2.4. Catalytic tests

The catalytic experiments were performed using a conventional system with a fixed bed quartz-reactor at atmospheric pressure. The feed composition was $EtOH/N_2 = 5/95$ molar ratio. The reaction temperature was varied in the range 300–450 ºC. The deactivation rate during the catalytic tests (4 h) was very low. Thus, the values of ethanol conversion (X,%) and the selectivity to main reaction products (S_i, %) were calculated considering the average values of the last 3 h of time on stream.

A typical reaction was performed as follows: the reactor charged with the catalyst was pre-heated at 120 °C, at this temperature the vaporized ethanol was fed and analysed with the on-line GC in order to evaluate the exact starting concentration of the reagent. After that, the temperature of the furnace was set to the desired reaction temperature and when reached, the reaction started. For each reaction, fresh new catalyst was loaded inside the reactor.

The reaction products were monitored by on-line gas chromatography (Agilent 7890 A) equipped with two capillary columns (Fig. S2): an HP-FFAP Polyethylene glycol (50 m x 320 μm x 0.5 μm) connected to a FID detector and a Rt-U-Bond (30 m x 530 μm x 20 μm) column connected to a TCD detector. The by-products were analysed by GC-MS (Agilent 6890 N system, equipped with a capillary HP-5MS (5%Phenyl Methyl Siloxane) (30 m x 250 μm x 0.25 μm) and coupled with Agilent 5973 N mass detector). Comprehensive explanation of compounds quantifications can be found in the electronic supporting information, SI.

Table 1
Physicochemical features of sepiolite supports.

Support	S^{a}_{BET} (m^2/g)	Acidity[b] NH_3-adsorbed (Desorption Temp.,°C)	Basicity[c] CO_2-adsorbed (Desorption Temp.,°C)	B/A[d]
MgO	41	nd	3	-
Sep@500	138	2.0 (180 °C; 260 °C; 350 °C)	1.8 (120 °C, 220 °C; 330 °C; 420 °C)	**0.92**
Sep@700	124	1.4 (180 °C; 260 °C; 350 °C)	1.2 (120 °C; 330 °C; 420 °C)	**0.83**

[a]) Determined by N_2 adsorption using BET technique.
[b]) Determined by TPD-NH_3 analysis (in $\mu mol_{NH3}/m^2$); in parenthesis temperature of desorption peaks.
[c]) Determined by TPD-CO_2 analysis (in $\mu mol_{CO2}/m^2$); in parenthesis temperature of desorption peaks.
[d]) Basicity/Acidity ratio.

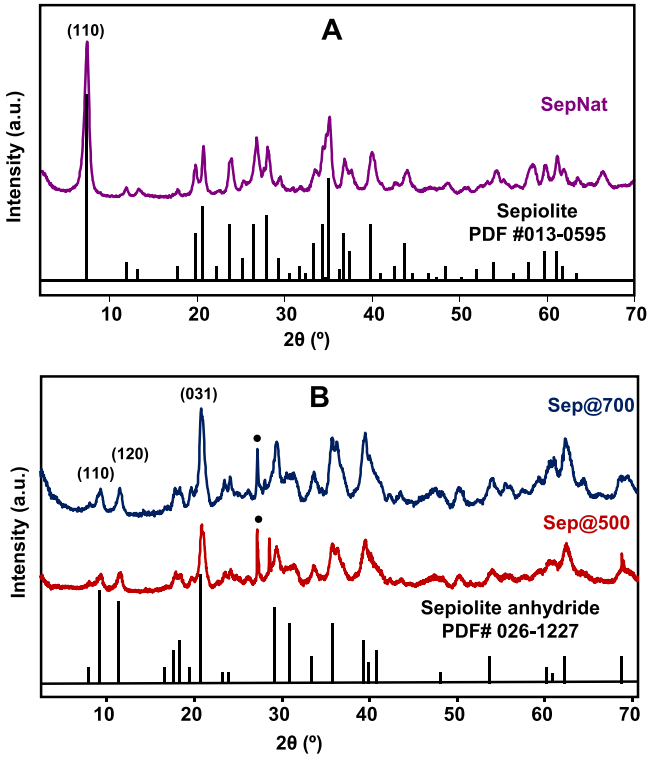

Fig. 1. XRD patterns of: A) Natural sepiolite sample (SepNat); B) Sepiolite calcined at 500ºC (Sep@500) or 700ºC (Sep@700). SA: Sepiolite Anhydride; Dot: quartz.

3. Results and discussion

3.1. Catalyst characterization

The main physicochemical features of the sepiolite supports and catalysts are summarized in Table 1.

The XRD patterns of sepiolite (Fig. 1A) showed that the main phase constituent of the raw material ("SepNat") was a well crystallized sepiolite, as indicated by the presence of the characteristic narrow and intense diffraction peak at 2θ= 7.3º, corresponding to the plane (110). Indeed, the XRD pattern of the raw material matched with the one of Sepiolite (Magnesium Silicate Hydroxide Hydrate, $Mg_4Si_6O_{15}(OH)_2{\cdot}8\ H_2O$, PDF# 00–013–0595).

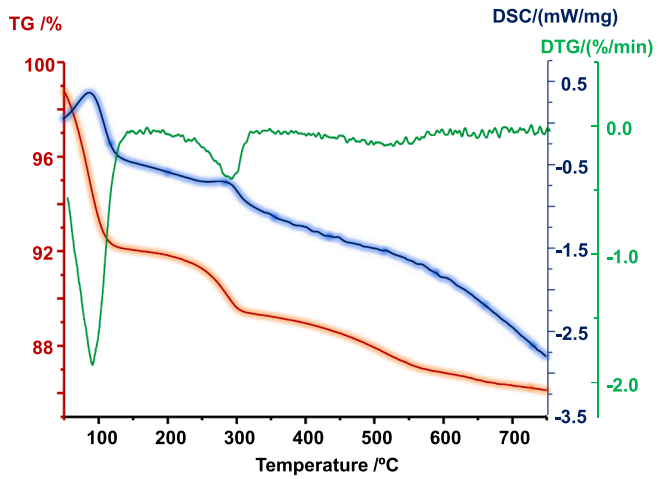

Fig. 2. TGA-DSC analysis of natural sepiolite sample.

Natural sepiolite has been calcined at 500 ºC (Sep@500) or at 700 ºC (Sep@700) for 3 h, with a 2ºC min^{-1} heating ramp. Upon thermal treatments, the peak at 7.31º disappeared, indicating that the layered structure of sepiolite collapsed with calcination. In fact, the XRD patterns of both calcined samples (i.e. Sep@500 and Sep@700) matched with the one of sepiolite anhydride (Magnesium Silicate Hydroxide, $Mg_8Si_{12}O_{30}(OH)_4$, PDF# 00–026–1227), revealing that the heating caused structural and textural changes associated with dehydration and dehydroxylation processes [46]. Furthermore, the slight increase with calcination temperature of the peaks intensity at ~8.9°,~11.1º and 20.25°, corresponding to the planes (110), (120) and (031) respectively (Fig. 1B) indicated the incremental formation of sepiolite anhydride with increasing temperature [46].

The TGA-DSC results (Fig. 2) confirmed the stepwise removal of water from Sepiolite with increasing temperature, which accounts for ~7.6% of the mass loss at 100 °C, for ~2.6% at 300 °C and for ~3.6% at 500ºC (all steps are endothermic processes as expected) with the total mass loss of ~14% by 800 °C. The dehydration steps corresponded to [47]: **i)** the loss of the weakly adsorbed water on the surface (i.e., adsorbed water and zeolitic water); **ii)** the loss of hydration water and; **iii)** the loss of coordination water.

The MgO sample, basic in nature, had a relatively low surface area of 41 $m^2\ g^{-1}$ in agreement with literature values [46,48]. The BET surface area of the two sepiolite samples calcined at 500 and 700 ºC were 138 $m^2\ g^{-1}$ and 124 $m^2\ g^{-1}$, respectively; showing a lower value of BET surface area at higher calcination temperature. The decrease in the surface area with increasing calcination temperature is a general phenomenon due to sintering of the samples at high temperatures.

The TPD profiles of calcined sepiolite samples are shown in Figs. S4 and S5, whereas the densities of acidic and basic sites, expressed as $\mu mol_{CO2}\ m^{-2}$ or $\mu mol_{NH3}\ m^{-2}$ are presented in Table 1. These results confirm that the density of both acidic and basic sites was higher for Sep@ 500, compared to the one calcined at 700 ºC. In addition, the basic/acid sites ratio (B/A) decreased from 0.92 to 0.83 while increasing the calcination temperature from 500 to 700 ºC, respectively. The differences in the acidic/basic properties between both sepiolite-based supports, calcined at different temperature, could be explained through the results of the XRD and TGA analysis performed over the natural sepiolite sample, shown in Figs. 1B and 2, respectively, where the formation of a new phase due to dehydration (i.e., Sepiolite anhydride) has been observed. Indeed, Mora et al. studied the effect of thermal treatment on sepiolite structure by means of IR analysis, finding a progressive removal of OH groups (of zeolitic water, Mg-OH groups and water octahedrally coordinated to magnesium) with increasing calcination temperature until 800 ºC, at which the layered structure of sepiolite collapsed and a new phase formed (estantite) [49]. Since

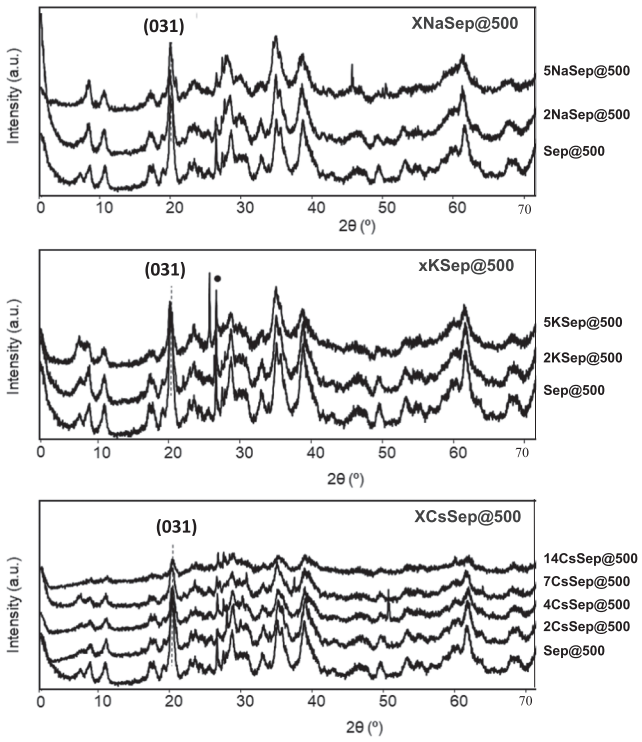

Fig. 3. XRD patterns of alkali metals-impregnated sepiolite samples (XMe/Sep@500). From top to bottom: sodium impregnated sepiolite samples (2 and 5 wt%); potassium impregnated sepiolite samples (2 and 5 wt%); cesium impregnated sepiolite samples (2, 4, 7 and 14 wt%).

exposed hydroxyl groups potentially can act both as Brønsted acid sites and basic sites, their changes in quantity during thermal treatment can be the cause of the acidity/basicity changes with increasing calcination temperature [50].

Metal loadings of 2 wt% and 5 wt% of Na were prepared with calcined sepiolite, calcined at 500ºC or 700ºC, while K (with K-loading of 2 or 5 wt%) and Cs (with Cs-loading of 2, 4, 7 or 14 wt%) were prepared only over the sepiolite support calcined at 500ºC, all by incipient wetness impregnation method. Fig. 3 reports the XRD patterns of the alkali metals-impregnated samples.

Thus, upon alkali deposition by IWI method, followed by calcination, a dispersion of metal oxides would be expected to be found on the catalyst surface. However, there were no indication of the presence of any new crystalline phases other than the sepiolite dehydrate, meaning a good dispersion of the metal oxide over the sepiolite surface has been obtained. Nevertheless, a partial degradation of the sepiolite structure has been observed. This could be confirmed by a decrease of the surface area with increasing metal loading (Table S2, Fig. S5). Additionally, this decrease may suggest the blockage of the narrower pores [51].

The main physicochemical features (specific surface area, actual metal loading, acidity, basicity and acidity/basicity ratio) of the catalysts after alkali metals impregnation with different metal loading are summarized in Table 2, in which the alkali metal loading is expressed as weight percentage (wt%) or as molar ratio over sepiolite weight ($mmol_{Metal}/g_{Ssepiolite}$).

Through the TPD analysis of probe molecules (i.e., NH_3 or CO_2), the acidic and basic features of the samples have been evaluated. It has been observed that the incorporation of small amount of alkali-metals in the natural sepiolite samples, pre-calcined at 500ºC, progressively neutralizes acid sites, as determined by the TPD of NH_3. In addition, the acidity/basicity ratio (A/B) has been computed. Indeed, the *n*-butanol selectivity from the ethanol Guerbet conversion has been found to be strictly related to the acid/base properties of the catalyst, in particular to their ratio [52,53]. More in detail, the highest *n*-butanol yields were associated to low ratio between acid and basic sites. A general decrease of the A/B ratio can be noticed with the presence of the alkali metals, linearly related with the extent of the amount added. As a consequence, a general increase of the overall basicity can be observed with increasing alkali metal loading.

It is known that base strength increases with the radius of alkali cations (Na^+= 227 pm, K^+= 280 pm, Cs^+= 343 pm) [54]. However, considering the samples containing the same amount of alkali metal added over sepiolite (i.e., ca. 0.6 $mmol_{Me}/g_{sep}$ in Table 2), neither the acidity nor the basicity followed a linear trend with increasing alkali metal ionic radius. Nevertheless, the same molar amount of the alkali metals corresponds to different metal weight loaded due to their diverse atomic mass, which could affect their dispersion over the sepiolite. Therefore, the variation of the acidic/basic properties observed could be related to the different alkali metal dispersion obtained. Nevertheless, no other phases or species have been detected through XRD analysis, meaning that they could be well dispersed over the catalyst surface. Thus, other characterization techniques should be needed to better understand the active sites structures (e.g. XPS, X-ray Absorption Fine Structure XAFS). However, linear decrease of the A/B ratio of the sepiolite samples can be noticed with increasing alkali-metal loading, so following the order $Na^+ < K^+ < Cs^+$.

3.2. Catalytic tests

Several blank tests were performed by feeding ethanol into the reactor, in the absence of the catalytic bed, in the range of the desired temperatures (250 – 450 °C), and no EtOH conversion have been

Table 2
Physicochemical features of alkali metals-based catalysts.

Catalyst	Alkali amount			S^b_{BET}	Acidity [c]	Basicity[d]	A/B[e]
	(wt%)	(mmol/g)	(mmol/g)[a]	(m^2/g)	($\mu mol_{NH3}/m^2$)	($\mu mol_{CO2}/m^2$)	
Sep@ 700	0	-	-	124	1.4	1.2	1.17
2Na/Sep@ 700	2	0.87	0.70	126	0.6	1.2	0.50
5Na/Sep@ 700	5	2.17	2.44	102	0.3	1.3	0.23
Sep@ 500	0	-	-	138	2.0	1.8	1.11
2Na/Sep@ 500	2	0.87	0.56	124	1.0	1.4	0.71
5Na/Sep@ 500	5	2.17	1.62	100	0.5	1.2	0.42
2 K/Sep@ 500	2	0.51	0.56	119	1.2	2.3	0.52
2 K/Sep@ 500	5	1.27	1.43	86	0.5	1.7	0.29
2Cs/Sep@ 500	2	0.15	0.12	130	1.6	0.3	5.33
4Cs/Sep@ 500	4	0.30	0.39	118	1.3	1.0	*1.30*
7Cs/Sep@ 500	7	0.53	0.59	110	1.0	1.6	*0.63*
14Cs/Sep@ 500	14	1.05	0.69	79	0.3	2.0	*0.15*

[a]) Determined by SEM-EDX analysis; [b]) Determined by nitrogen adsorption using BET technique; [c]) NH_3 desorption, determined by TPD-NH_3; (in $\mu mol_{NH3}/m^2$); [d]) CO_2-desorption, determined by TPD-CO_2 (in $\mu mol_{CO2}/m^2$); [e]) Basicity/Acidity ratio.

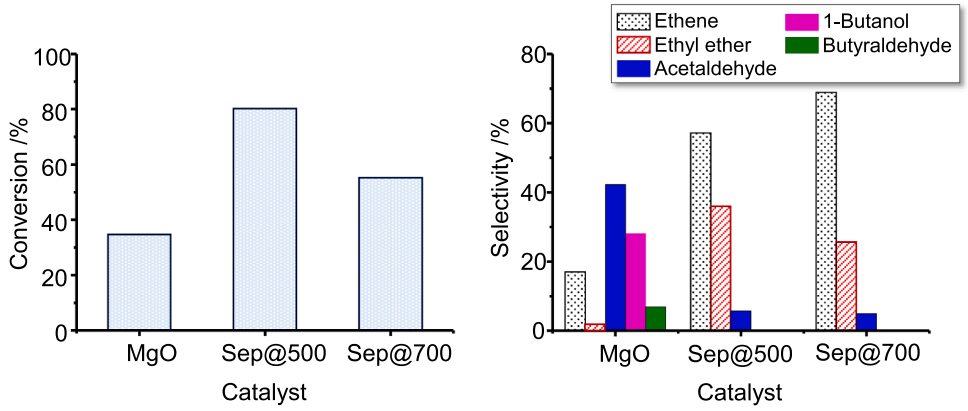

Fig. 4. Ethanol conversion (left) and selectivity to the main reaction products (right), during the ethanol transformation over MgO, Sep@ 500 and Sep@ 700 catalysts. Reaction conditions: EtOH 5% v/v in N_2, T = 450 °C, P = 1 atm, WHSV= 1 $g_{ETOH}/(g_{CAT}•h)$.

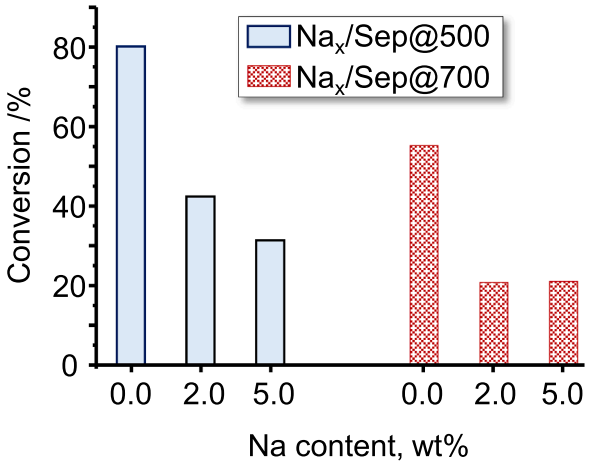

Fig. 5. Ethanol conversion (X,%) for the ethanol gas-phase transformation over Na-doped sepiolite catalysts: xNa/Sep@ 500 and xNa/Sep@ 700 series, with Na-loading (x) of 0, 2 or 5 wt%. Reaction conditions: EtOH 5% v/v in N_2, T = 450 °C, P = 1 atm, WHSV= 1 $g_{ETOH}/(g_{CAT}•h)$. Catalysts: Sep@ 500, 2Na/Sep@ 500, 5Na/Sep@ 500, Sep@ 700, 2Na/Sep@ 700 and 5Na/Sep@ 700.

detected along the temperature range evaluated. Then, the catalytic activity of the calcined supports (i.e., Sep@500 and Sep@700) has been tested and compared to the one obtained with the reference catalysts, MgO, previously synthetized in the lab. The tests have been carried out at 450 °C, with a percentage of EtOH in the feed stream equal to 5 mol% in N_2 while keeping a weight hourly space velocity (WHSV) of 1 $g_{ETOH}/(g_{CAT}$ h). The results, expressed in terms of conversion of EtOH, as well as the selectivity to the main reaction products ($_{Si}$), are shown in Fig. 4.

It can be noted that the sepiolite supports, i.e. Sep@ 500 and Sep@ 700, are more active compared to MgO (Fig. 4), leading to a higher ethanol conversion values, equal to 80%, 55% and 35%, respectively. Moreover, the thermally treated sepiolite samples mainly performed as acid catalysts leading to the formation of the dehydration products of ethanol, namely diethyl ether and ethene. In addition, the sepiolite sample calcined at 700 °C was less active than the one treated at 500 °C; the lower activity mainly related to the lower value of surface area of Sep@ 700 sample (see Table 1).

One possible way to decrease the dehydration rate of ethanol over sepiolite is to selectively remove, block or deactivate the acid sites responsible for dehydration by adding small amounts of alkali metal. Figs. 5 and 6 summarizes the catalytic results obtained over the Na-doped samples.

As it can be seen in Fig. 5, the sodium addition over sepiolite resulted in a generalized reduction in activity, leading to lower values of ethanol conversion, in both xNa/Sep@ 500 and xNa/Sep@ 700 series.

At the same time, the selectivity of ethanol dehydration products

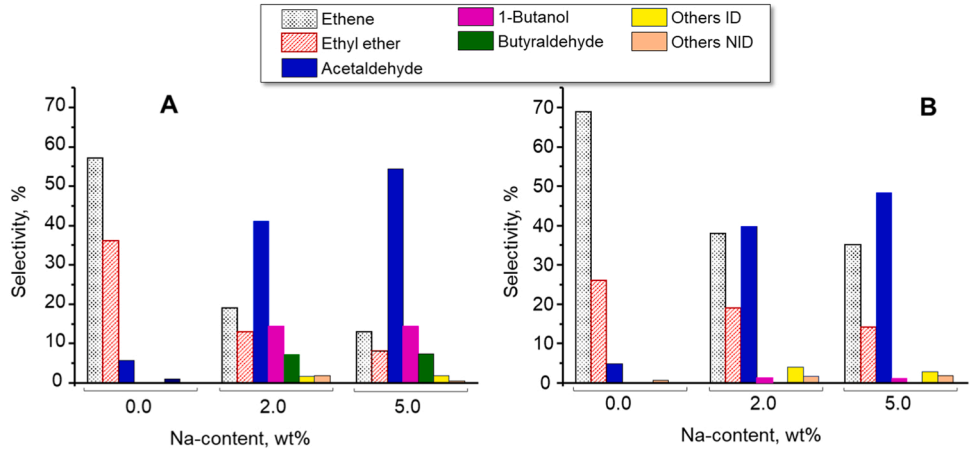

Fig. 6. Influence of Na-content on the selectivity of the main reaction products (S_i, %), during the ethanol gas-phase transformation over Na-doped sepiolite catalysts: A) xNa/Sep@ 500; and B) xNa/Sep@ 700 series, with Na-loading (x) of 0, 2 or 5 wt%. Others ID: acetone, 2-pentanone, CO_2, ethane; Others NID: other unidentified products. Reaction conditions as in Fig. 5.

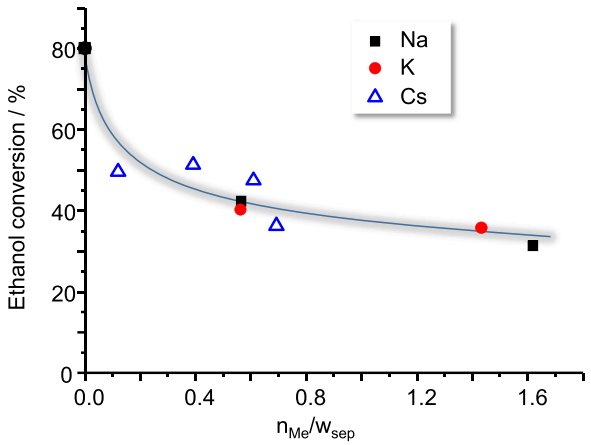

Fig. 7. Influence of alkali metal loading n_{Me}/w_{sep} ($mmol_{Me}/g_{sep}$, measured by SEM-EDX) on the conversion of the ethanol. Reaction conditions: EtOH 5% v/v in N_2, Temperature= 450 °C; P = 1 atm; WHSV= 1 $g_{EtOH}/(g_{CAT}•h)$. Catalysts: 2Na and 5Na/Sep@ 500; 2 K and 5 K/Sep@ 500; 2Cs, 4Cs, 7Cs and 14Cs/Sep@ 500.

(ethene and diethyl ether) decreased while selectivity of the reaction product of ethanol dehydrogenation (acetaldehyde) increased with Na metal loading (Fig. 6). This can be related to the change of acid-base properties of the catalysts, as determined by TPD analysis (Table 2, Figs. S3 and S4), where it has been observed a decrease of the acidity with increasing alkali-metal loading. Interestingly, over the Sep@ 700 supported samples in addition of being less active, the extent of the decreasing of acid reaction products (Fig. 6B) was lower than the one obtained over the Sep@ 500 supported samples (Fig. 6A). The overall selectivity of diethyl ether and ethene decreased from ~95% for the support alone to ~ 50% with 5 wt% of sodium for the sepiolite calcined at 700ºC, while it decreased from ~95% to ~20% for the one supported over Sep@ 500.

Noteworthy the Na-modified Sep@ 500 supported catalysts led to the formation of the Guerbet reaction product of ethanol: *n*-butanol. Indeed, the 2Na/Sep@ 500 catalyst allowed to obtain *n*-butanol with a selectivity of 14%. An increase of the alkali metal loading did not lead to any beneficial effects, showing lower conversion with steady *n*-butanol selectivity.

The presence of an alkali metal showed to be crucial in favouring the *n*-butanol formation pathway. Its presence led to an overall decrease of the sepiolite acidity probably generating the right acidity/basicity ratio required to induce *n*-butanol formation [46,47]. Accordingly, in order to evaluate the effect of bigger and more electropositive alkali metals, other sepiolite-supported catalysts have been prepared with different alkaline metals. In particular, potassium and cesium have been added through incipient wetness impregnation with different metal loading (i.e., 2, 4, 5, or 14 wt%) over previously calcined sepiolite at 500ºC. All the samples have been tested into the reaction system by feeding EtOH 5% v/v in N_2 at 450 °C, P = 1 atm and WHSV= 1 $g_{ETOH}/(g_{CAT}•h)$. Fig. 7 summarizes the catalytic results obtained enlightening the dependence of ethanol conversion (X,%) and main products selectivity (S, %) on the molar alkali metal loading, expressed as moles of the metals (mmol) divided by the weight of the sepiolite (g), $n_{Metal}/w_{sepiolite}$. Here, the catalytic results are reported in relation to the measured alkali metals amount by SEM-EDX analysis (See Table 2).

According to these results, it is possible to propose a trend for both ethanol conversion (Fig. 7) and the distribution of the main reaction products (Fig. 8) with the molar amount of the alkali metals over sepiolite support (highlighted by the dotted line). Ethanol conversion and the selectivity to the dehydration products (i.e. ethene and diethyl ether) decreased with increasing alkali-metal amount, showing a linear correlation between activity and acidity.

In an opposite trend, acetaldehyde selectivity increased when the

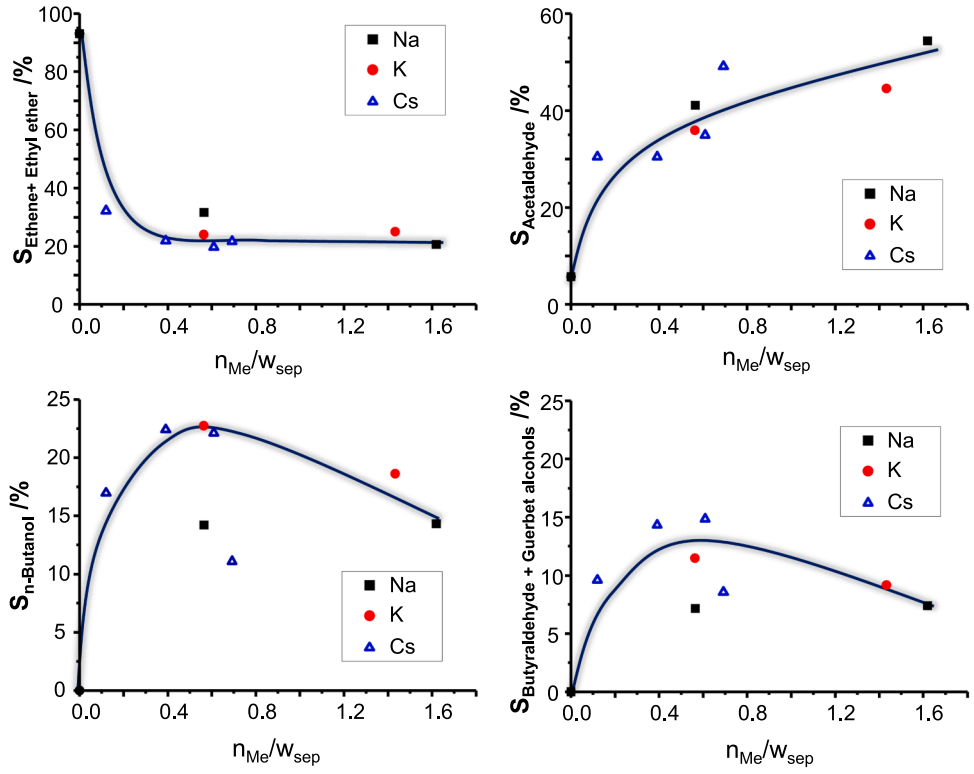

Fig. 8. Influence of alkali metal loading n_{Me}/w_{sep} ($mmol_{Me}/g_{sep}$, measured by SEM-EDX) on the selectivity to the main reaction products. Guerbet alcohols: 2-ethyl-butanol, 1-hexanol, 2-ethyl-hexanol, 1-octanol. Reaction conditions: EtOH 5% v/v in N_2, Temperature= 450 °C; P = 1 atm; WHSV= 1 $g_{EtOH}/(g_{CAT}•h)$. Catalysts: 2Na and 5Na/Sep@ 500; 2 K and 5 K/Sep@ 500; 2Cs, 4Cs, 7Cs and 14Cs/Sep@ 500.

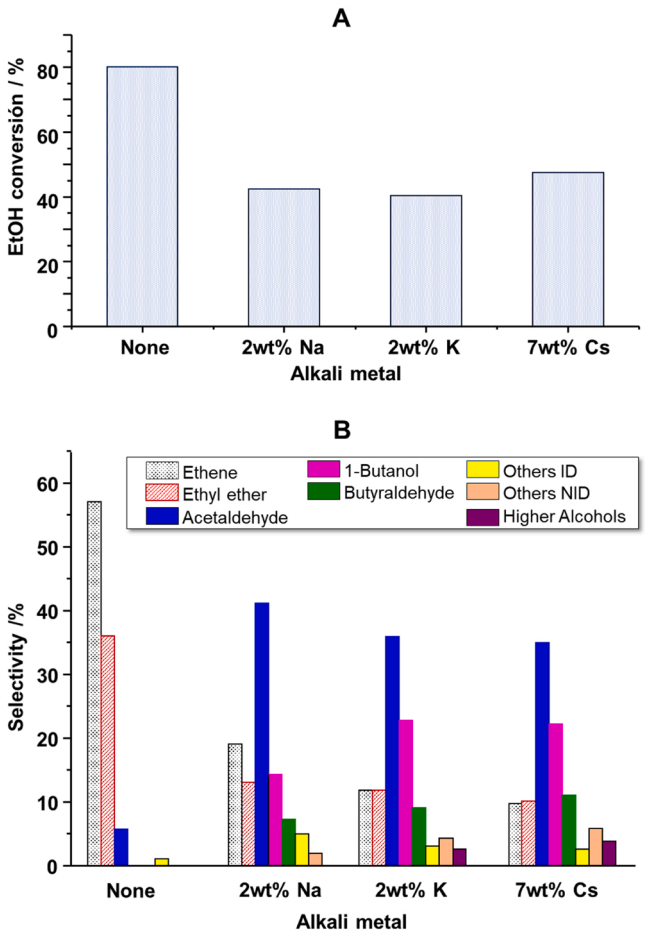

Fig. 9. Conversion of the ethanol (A) and the selectivity of the main reaction products (B) over the alkali-metal doped catalyst with ~0.6 $mmol_{Me}/g_{sep}$ of molar metal loading (n_{Me}/w_{sep}). Guerbet alcohols: 2-ethyl-butanol, 1-hexanol, 2-ethyl-hexanol, 1-octanol. Reaction conditions: EtOH 5% v/v in N_2, P = 1 atm, Temperature= 450 °C; WHSV= 1 $g_{EtOH}/(g_{CAT}•h)$. Catalysts: 2Na/Sep@ 500; 2 K/Sep@ 500; 7Cs/Sep@ 500.

alkali-metal loading increased (Fig. 8). However, the trends of *n*-butanol selectivity as well as the selectivity to butyraldehyde and higher alcohols, is affected by both the nature and the amount of the alkali metal. Indeed, both the trends of *n*-butanol and the consecutive Guerbet higher alcohols selectivity presented a maximum in relation with the alkali metal loading. The maximum value of *n*-butanol selectivity was obtained around 22% over the 2 K/Sep@ 500 and 7Cs/Sep@ 500 catalysts, which contained the same molar amount of alkali metal (namely ~0.6 $mmol_{Me}/g_{sep}$). It is worth noting that the acidity/basicity ratio (A/B ratio) measured by TPD analysis for both catalysts was quite similar (i.e. 0.52 and 0.63, respectively).

Fig. 9 highlights the effect of the nature of the alkali metal over the EtOH conversion (Fig. 9A) and the selectivity to the main products (Fig. 9B) obtained over the catalysts containing ca. 0.6 $mmol_{Me}/g_{sep}$ (i.e. 2Na/Sep@500, 2 K/Sep@500 and 7Cs/Sep@500 catalysts). These catalysts are the ones which led to achieve the highest selectivity to *n*-butanol, ca. 22%. As far as the dehydration products formation is concerned, bigger alkali metal atom led to effectively decrease their production, following the trends $Na^+ > K^+ > Cs^+$, in accordance with the lower acidity of the catalyst. In addition, it can be noted that the Cs-containing sample favored the formation of higher alcohols and butyraldehyde. In summary, the best results in terms of activity ($X_{EtOH=}$ 47%) and *n*-butanol selectivity (S_{BuOH}: 22%) and yield (10%), have been obtained with the 7Cs/Sep@ 500 catalyst.

Considering that the best performance, in terms of *n*-butanol yield, has been obtained over the 7Cs/Sep@ 500 catalyst, this catalyst has been employed to further investigate the effects of some reaction parameters on the catalyst activity. In particular, the reaction temperature (T_R, °C) and weight hourly space velocity (WHSV, $g_{EtOH}/(g_{CAT}•h)$) have been investigated in order to find the optimal conditions for *n*-butanol formation. To do so, catalytic tests have been performed at a reaction temperature of 400 or 450 °C and in the WHSV range of 0.11–2.0 $g_{ETOH}/(g_{CAT}•h)$ (Fig. S6).

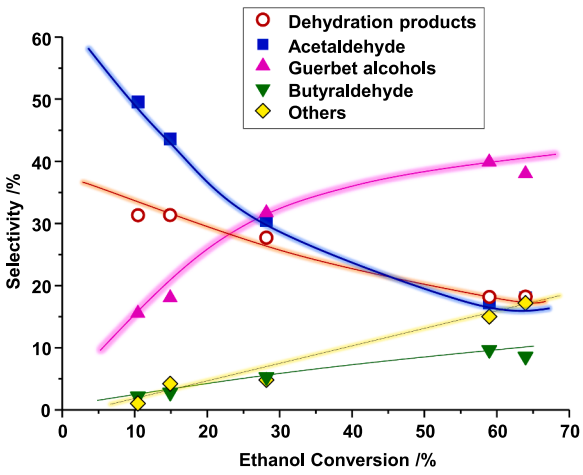

Fig. 10. Variation of the selectivity to the main reaction products (S_i, %) with ethanol conversion over the 7Cs/Sep@ 500 catalyst. Guerbet alcohols: n-butanol, 2-ethyl-butanol, 1-hexanol, 2-ethyl-hexanol, 1-octanol; Others: others NID (Other unidentified products) and ID (acetone, 2-pentanone, CO_2, ethyl acetate, ethane). Reaction conditions: EtOH 5% v/v in N_2, Temperature= 400 °C; P = 1 atm; WHSV= 2, 1, 0.3, 0.2 and 0.1 $g_{EtOH}/(g_{CAT}•h)$.

It has been observed an increasing trend of the ethanol conversion with both the reaction temperature and the WHSV, as expected. On the other hand, the products distribution has been differently affected by those reaction parameters. In particular, when the influence of the contact time (W/F) was evaluated at 400 °C, the selectivity of *n*-butanol reached a plateau around 30% with a W/F of 0.3 $g_{ETOH}/(g_{CAT}•h)$ (Fig. S6). Moreover, while investigated at higher temperature (i.e., 450°C), a decreasing trend of the W/F led to lower value of *n*-butanol selectivity (Fig. S6), probably due to its conversion into consecutive reaction products. Indeed, an opposite increasing trend for both the Others-ID and Other-NID products has been observed. From GC-MS analysis it has been observed their main nature as aromatics and longer chain ketones (i.e., 4-nonanone and 4-undecanone). Nevertheless, the best reaction conditions in terms of *n*-butanol selectivity (30%), corresponding to a total *n*-butanol yield of 18%, have been found to be as follows: 400°C, W/F of 0.2 $g_{ETOH}/(g_{CAT}•h)$.

In addition, from the point of view of the overall Guerbet alcohols production, Fig. 10 presents the variation of the selectivity to the main reaction products with the ethanol conversion for the 7Cs/Sep@ 500 catalyst. For comparison, Fig. S7 presents the variation of ethanol conversion with contact time, W/F (in $g_{CAT}/(mL·s)$). As it can be observed in Fig. 10, the total alcohols selectivity followed the same trends manifested by 1-butanol, reaching a maximum of the cumulative selectivity of Guerbet alcohols as high as 40% with an ethanol conversion of 60%, while working in the optimized reaction conditions, i.e., 400 °C, and WHSV of 0.2 $g_{ETOH}/(g_{CAT}•h)$.

4. Conclusions

In this paper, the continuous upgrading of EtOH to *n*-butanol and higher alcohols over calcined sepiolite promoted by alkali metals has been demonstrated with good results both in terms of ethanol conversion and *n*-butanol yield compared to the results recently reported in

continuous-flow reactions (see Fig. S8). Indeed, a relative high *n*-butanol yield (18%) was obtained at 400ºC reaction temperature and WHSV 0.2 $g_{ETOH}/(g_{CAT}•h)$ with 7 wt% of Cs metal loading over the sepiolite calcined at 500ºC. It is worth noting that the cumulative selectivity of *n*-butanol and higher Guerbet alcohols, which find suitability for advanced biofuel and lubricants applications, was 40%, corresponding to a total yield of ~24%.

The results here reported are of interest since, from the perspective of the "Green and Sustainable Development" concept, the use of naturally abundant clay minerals like sepiolite as catalyst has economical, eco-friendly and nontoxic advantages [55]. In this study, sepiolite has been used for the first time as heterogeneous catalyst for performing ethanol gas-phase Guerbet conversion into higher alcohols with reasonable yields, opening new perspectives for future catalyst engineering for this kind of complex reaction mechanism.

CRediT authorship contribution statement

Giulia Balestra: Methodology, Investigation, Data curation, Writing – review & editing. **Jacopo de Maron:** Investigation, Data curation. **Tommaso Tabanelli:** Methodology, Data curation, Writing – review & editing, Supervision. **Fabrizio Cavani:** Conceptualization, Writing – review & editing, Supervision. **Josè Manuel López Nieto:** Conceptualization, Resources, Data curation, Writing – review & editing, Supervision.

Declaration of Competing Interest

The authors declare that they have no known competing financial interests or personal relationships that could have appeared to influence the work reported in this paper.

Data availability

The data that has been used is confidential.

Acknowledgments

The authors would like to acknowledge the Ministerio de Ciencia e Innovación of Spain (TED2021-130756B-C31).

Appendix A. Supplementary material

Supplementary data associated with this article can be found in the online version at doi:10.1016/j.cattod.2023.01.020.

References

[1] D. Martin Alonso, J.Q. Bond, A.J. Dumesic, Green Chem. 12 (2010) 1493–1513.
[2] R.F. Service, Science 329 (2010) 784–785.
[3] C.A. Cardona, O.J. Sánchez, Bioresour. Technol. 98 (2007) 2415–2457.
[4] L. Panella, Sugar Tech 12 (2010) 288–293.
[5] C.S. Goh, K.T. Lee, Renew. Sustain. Energy Rev. 14 (2010) 842–848.
[6] R.P. John, G.S. Anisha, K.M. Nampoothiri, A. Pandey, Bioresour. Technol. 102 (2011) 186–193.
[7] M.Y. Menetrez, Environ. Sci. Technol. 46 (2012) 7073–7085.
[8] V. Menon, M. Rao, Prog. Energy Combust. 38 (2012) 522–550.
[9] R.C. Saxena, D.K. Adhikari, H.B. Goyal, Renew. Sustain. Energy Rev. 13 (2009) 167–178.
[10] A. Singh, P.S. Nigam, J.D. Murphy, Bioresour. Technol. 102 (2011) 10–16.
[11] J.O.B. Carioca, Biotechnol. J. 5 (2010) 260–273.
[12] B.G. Harvey, H.A. Meylemans, Chem. Technol. Biotechnol. 86 (2011) 2–9.
[13] C. Yang, Z.Y. Meng, J. Catal. 142 (1993) 37–44.
[14] Ed. Kirk-Othmer Encyclopedia of Chemical Technology, John Wiley & Sons, 2001.
[15] A.S. Ndou, N. Plint, N. Coville, J. Appl. Catal. A 251 (2003) 337–345.
[16] E.M. Green, Curr. Opin. Biotechnol. 22 (2011) 337–343.
[17] C. Jin, M. Yao, H. Liu, C.F.F. Lee, J. Ji, Renew. Sustain. Energy Rev. 15 (2011) 4080–4106.
[18] R.E. Miller, G.E. Bennett, Patent US353233A, assigned to Monsanto Chemicals Ltd 1956.
[19] A.J. O'Lenick, J. Surfactants Deterg. 4 (2001) 311–315.
[20] C. Cesari, A. Gagliardi, A. Messori, N. Monti, V. Zanotti, S. Zacchini, I. Rivalta, F. Calcagno, C. Lucarelli, T. Tabanelli, F. Cavani, R. Mazzoni, J. Catal. 405 (2022) 47–59.
[21] L. Izzo, T. Tabanelli, F. Cavani, P. Blair Vàsquez, C. Lucarelli, M. Mella, Catal. Sci. Technol. 10 (2020) 3433–3449.
[22] R. Mazzoni, C. Cesari, V. Zanotti, C. Lucarelli, T. Tabanelli, F. Puzzo, F. Passarini, E. Neri, G. Marani, R. Prati, F. Viganò, A. Conversano, F. Cavani, ACS Sustain. Chem. Eng. 7 (1) (2019) 224–237.
[23] J. De Maron, M. Eberle, F. Cavani, F. Basile, N. Dimitratos, P.J. Maireles-Torres, E. Rodriguez-Castellón, T. Tabanelli, ACS Sustain. Chem. Eng. 9 (4) (2021) 1790–1803.
[24] Y. Xie, Y. Ben-David, L.J.W. Shimon, D. Milstein, J. Am. Chem. Soc. 138 (2016) 9077–9080.
[25] J. Campos-Fernández, J.M. Arnal, J. Gómez, M.P. Dorado, Appl. Energy 95 (2012) 267–275.
[26] C.F. de Graauw, J.A. Peters, H. van Bekkum, J. Huskens, Synthesis 1994 (10) (1994) 1007–1017.
[27] T. Tabanelli, Curr. Opin. Green Sustain. Chem. 29 (2021), 100449.
[28] D. Gabriëls, W.Y. Hernández, B. Sels, P.V.D. Voort, A. Verberckmoes, Catal. Sci. Technol. 5 (2015) 3876–3902.
[29] A. Chieregato, J. Velasquez Ochoa, C. Bandinelli, G. Fornasari, F. Cavani, M. Mella, ChemSusChem 8 (2015) 377–388.
[30] L. Silvester, J.-F. Lamonier, C. Lamonier, M. Capron, R.-N. Vannier, A.-S. Mamede, F. Dumeignil, ChemCatChem 9 (2017) 2250–2261.
[31] H. Aitchison, R.L. Wingad, D.F. Wass, ACS Catal. 6 (2016) 7125–7132.
[32] W. Ueda, T. Ohshida, T. Kuwabara, Y. Morikawa, Catal. Lett. 12 (1992) 97–104.
[33] A.S. Ndou, N. Coville, J. Appl. Catal. A 275 (2004) 103–110.
[34] J.T. Kozlowski, R.J. Davis, ACS Catal. 3 (2013) 1588–1600.
[35] T. Tsuchida, J. Kubo, T. Yoshioka, S. Sakuma, T. Takeguchi, W. Ueda, J. Catal. 259 (2008) 183–189.
[36] S. Hanspal, Z.D. Young, H. Shou, R.J. Davis, ACS Catal. 5 (2015) 1737–1746.
[37] J.I. Di Cosimo, C.R. Apesteguıa, M.J.L. Ginés, E. Iglesia, J. Catal. 190 (2000) 261–275.
[38] I.-C. Marcu, N. Tanchoux, F. Fajula, D. Tichit, Catal. Lett. 143 (2013) 23–30.
[39] B. Nagy, W. Bradle, Am. Mineral. 40 (1955) 885–892.
[40] A.J. Dandy, M.S. Nadiye-Tabbiruka, Clays Clay Miner. 30 (1982) 347–352.
[41] Y. Kitayama, A. Abe, Nippon Kagaku Kaishi 1989 (1989) 1824–1829.
[42] A.A. Berenguer, C.B. Martin, US Patent US5051202A, assigned to Tolsa SA, 1991.
[43] D.K. Dutta, Developments in clay science, in: R. Schoonheydt, C.T. Johnston, F. Bergaya (Eds.), Surface and Interface Chemistry of Clay Minerals Vol. 9, Elsevier, 2018, pp. 289–329.
[44] G. Tian, G. Han, F. Wang, J. Liang, Nanomaterials from clay minerals, in: A. Wang, W. Wang (Eds.), Micro and Nano Technologies, Elsevier, 2019, pp. 135–201.
[45] A. Corma, J.M. López Nieto, N. Paredes, J. Catal. 144 (1993) 425–438.
[46] N. Yener, M. Önal, G. Üstünışık, Y. Sarıkaya, J. Therm. Anal. Calorim. 88 (2007) 813–817.
[47] B.M. Nagaraja, V. Siva Kumar, V. Shashikala, A.H. Padmasri, S. Sreevardhan Reddy, B. David Raju, K.S. Rama Rao, J. Mol. Catal. A 223 (2004) 339–345.
[48] P. Putanov, E. Kis, G. Boskovic, K. Lázár, Appl. Catal. 73 (1991) 17–26.
[49] M. Mora, M.I. López, M.A. Carmona, C. Jiménez-Sanchidrián, J.R. Ruiz, Polyhedron 29 (2010) 3046–3051.
[50] G. Busca, Phys. Chem. Chem. Phys. 1 (1999) 723–736.
[51] A. Walczyk, A. Michalik, B.D. Napruszewska, J. Kryściak-Czerwenka, R. Karcz, D. Duraczyńska, R.P. Socha, Z. Olejniczak, A. Gaweł, A. Klimek, M. Wójcik-Bania, K. Bahranowski, E.M. Serwicka, Appl. Clay Sci. 195 (2020), 105740.
[52] Z. Sun, A. Couto Vasconcelos, G. Bottari, M.C.A. Stuart, G. Bonura, C. Cannilla, F. Frusteri, K. Barta, ACS Sustain. Chem. Eng. 5 (2017) 1738–1746.
[53] L. Silvester, J.-F. Lamonier, J. Faye, M. Capron, R.-N. Vannier, C. Lamonier, J.-L. Dubois, J.-L. Couturier, C. Calais, F. Dumeignil, Catal. Sci. Technol. 5 (2015) 2994–3006.
[54] K. Gotoh, S. Nakamura, T. Mori, Y. Morikawa. Studies in Surface Science and Catalysis Vol. 130, Elsevier, 2000, pp. 2669–2674.
[55] J. Baloyi, T. Ntho, J. Moma, RSC Adv. 8 (2018) 5197–5211.